J. Astrophys. Astr. (2020) 41:43
https://doi.org/10.1007/s12036-020-09661-8

Recurrent novae: Single degenerate progenitors of Type Ia supernovae

G. C. ANUPAMA* and M. PAVANA

Indian Institute of Astrophysics, II Block Koramangala, Bengaluru 560 034, India.
*Corresponding author. E-mail: gca@iiap.res.in

MS received 15 September 2020; accepted 19 October 2020

Abstract. Type Ia supernovae are the result of explosive thermonuclear burning in CO white dwarfs. The progenitors of the Ia supernovae are white dwarfs in an interacting binary system. The donor companion is either a degenerate star (white dwarf) or a non-degenerate star (e.g. red giant). Recurrent novae are interacting binaries with a massive white dwarf accreting from either a main sequence, slightly evolved, or a red giant star. The white dwarf in these systems is a massive, hot white dwarf, accreting at a high rate. Recurrent novae are thought to be the most promising single degenerate progenitors of Type Ia supernovae. Presented here are the properties of a few recurrent novae based on recent outbursts. The elemental abundances and their distribution in the ejected shell are discussed.

Keywords. Type Ia supernovae—recurrent novae—abundances.

1. Introduction

1.1 *Type Ia supernovae*

Type Ia supernovae (SNe Ia) are the result of explosive thermonuclear burning in CO white dwarfs (WDs). The outcome of the explosive CO fusion leads to an ejecta structure in which iron group elements (IGE), including ^{56}Ni, make up the inner regions, surrounded by Si-rich outer layers. The distinguishing feature of SNe Ia spectra is the lack of hydrogen features, and the prominent Si II absorption features at maximum. The peak luminosity is dependent on the amount of ^{56}Ni synthesised during the explosion and the rate of decline is correlated with the peak luminosity, with brighter slower and fainter faster events (Phillips 1993). This correlation makes SNe Ia good standardizable candles for cosmology. In addition, SNe Ia are responsible for more than half the iron in the Solar neighbourhood (Maoz & Graur 2017).

Diversity in SNe Ia has become apparent in recent times with the increase in the discovery and detailed studies of these objects. It is found that nearly 30% of the events do not follow the Phillips relation. The diversity in the observed properties have given rise to the possibilities of (a) different mechanisms for the explosion, and (b) different progenitors. Theoretical modelling, combined with observational data, indicate the likely scenarios for the explosion are the delayed detonation (deflagration-to-detonation) of a Chandrasekhar mass WD (Khokhlov 1991) where the propagating nuclear flame starts off as a subsonic deflagration and transitions to a supersonic detonation at a critical density; or a prompt detonation (double-detonation) in a sub-Chandrasekhar mass WD (Woosley & Weaver 1994). The most promising progenitor binary systems are: (i) a Chandrasekhar mass white dwarf accreting matter in a single degenerate system (delayed detonation); (ii) a sub-Chandrasekhar WD that is accreting helium-rich material through Roche-lobe overflow, exploding via double detonation; or (iii) a double white dwarf merger where mass transfer happens on a dynamical timescale. The explosion mechanism in the case of WD mergers could be delayed detonation on a Chandrasekhar WD, or double detonation on a sub-Chandrasekhar WD.

This article is part of the Topical Collection: Chemical elements in the Universe: Origin and evolution.

Published online: 14 December 2020

Early observations may allow us to test whether SNe Ia arise from single degenerate, double degenerate or super/sub-Chandrasekhar scenarios. In the case of the single degenerate systems, early photometric observations should reveal signatures of collision of supernova with its companion (Kasen 2010). Prompt spectroscopic observations will reveal signatures of the circumstellar material, which could be due to the mass loss from the companion in single degenerate systems, or due to the common envelope in the double degenerate systems. UV flash was observed in the young Ia event iPTF14atg (Cao *et al.* 2015), while narrow absorption systems due to Ca II H&K, Na I, Fe II, Ti II, He I and Balmer lines blue shifted at $100-65\,\mathrm{km\,s^{-1}}$ were detected in the early phase observations of the PTF11kx (Patat *et al.* 2011; Dilday *et al.* 2012). These absorption systems are very similar to the ones seen in nova systems with a red giant companion such as the recurrent nova RS Ophiuchi.

1.2 *Recurrent novae*

A nova is an interacting binary system where the primary is a WD accreting material from a main sequence companion. Nova outbursts are due to a thermonuclear runaway reaction occurring at the base of the accretion disc (Starrfield *et al.* 2012). The outbursts are accompanied by ejection of the accreted matter. Novae with more than one recorded outburst are referred to as Recurrent Novae (RNe). The outbursts occur at intervals ranging from as short as one year to several decades. There are 10 confirmed RNe in our Galaxy, one in M31 and about two in the Large Magellanic Cloud, making these systems relatively rare systems (Schaefer 2010; Anupama 2013). The critical accreted mass required to trigger a thermonuclear runaway is lower for a high mass WD with high surface gravity. Therefore, RNe are expected to occur on hot WDs that are near the Chandrasekhar mass limit, accreting at a high rate. Theoretical studies (and observational inferences) have shown that the WD in these systems are gaining mass, making them good candidates for being the progenitors of Type Ia supernova (Starrfield *et al.* 2020).

We discuss here a few recurrent nova systems based on their recent outbursts, in particular the elemental abundances and distribution in the ejected material. Optical spectra of four Galactic and one extragalactic recurrent novae are used to obtain the abundance values in the ejecta using the plasma simulation and spectral synthesis code, CLOUDY (Ferland *et al.* 2017). Also obtained are the 3D morphology of their ejecta using pyCloudy (Morisset 2013). The 3D structure of the ejecta provide a spatial distribution of elements in the nova shell.

2. RS Ophiuchi

Recurrent nova RS Oph underwent its sixth recorded outburst on 2006 Feb 12.83 UT (Narumi *et al.* 2006). The fifth and the sixth outbursts were studied in detail from X-rays to radio wavelength regions. The multi-wavelength analyses clearly showed the evidence of shock interaction in this system, such as detection of evolution of blast wave in X-rays (Bode *et al.* 2006; Sokoloski *et al.* 2006), decrease in the spectral line width (expansion velocity) in optical and NIR (Skopal *et al.* 2008; Mondal *et al.* 2018), and low-frequency synchrotron emission in radio (Kantharia *et al.* 2007).

Detailed temporal evolution of the optical spectra along with the evolution of physical conditions in the ejecta from outburst to immediate post-outburst quiescence was studied by Mondal *et al.* (2018). The early phase spectrum shows permitted lines. By day 15, high excitation and coronal lines begin to appear. The strength of these lines intensify, and reach a peak coincident with the supersoft phase. The intensity of these lines fade as the nova enters the nebular phase. The abundance estimates obtained for different epochs by Mondal *et al.* (2018) using CLOUDY are given in Table 1. The abundances of the all the elements listed are found to be overabundant as compared. A temporal variation is seen in the estimated abundances due to temporal variations in the physical conditions,

Table 1. Chemical abundance values of the RS Oph ejecta at different epochs.

Day	9	12	28	50	103	159	189	249
$He/He_\odot$	1.70	1.75	1.80	1.90	2.50	2.00	1.60	1.60
$N/N_\odot$	–	–	11.0	12.0	10.0	5.0	8.0	3.0
$O/O_\odot$	–	–	1.0	1.0	5.0	0.7	0.3	0.3
$Ne/Ne_\odot$	1.9	2.0	2.0	2.5	5.0	1.0	0.7	0.5
$Ar/Ar_\odot$	–	4.0	4.9	5.2	5.5	–	–	–
$Fe/Fe_\odot$	2.7	2.8	3.0	3.5	3.8	0.5	0.5	0.5
$S/S_\odot$	–	–	–	–	1.0	1.5	–	1.5
$Ni/Ni_\odot$	1.5	1.8	2.0	2.0	2.0	–	–	–

Abundance values are given in the logarithmic scale, relative to hydrogen.

such as density and temperature, in the nova ejecta as it expands. A study of the quiescence spectrum by Mondal *et al.* (2020) indicates helium to be subsolar, while iron is over abundant.

The morphology of the ejecta was obtained using pyCloudy and the best-fit physical parameters obtained by Mondal *et al.* (2018) on days 50 and 159. It was found to be bipolar with equatorial rings and cones (Figure 1). The [O III] lines are coming from the outermost regions of the equatorial rings while Fe II are coming from the innermost rings. [N II] are originating from the conical base while He I and He II from the inner regions of the cones. The coronal lines are from the outer most regions surrounding rings and cones. The inclination angle of the system was found to be $44^\circ \pm 0.85^\circ$.

3. V3890 Sgr

V3890 Sgr underwent its third recorded outburst on 2019 Aug 27.87 UT (Pereira 2019, VSNET-Alert 23505). Emission from γ-rays to radio have been detected during this outburst. Similar to RS Oph, evidence for shock interaction of the ejecta with the red giant wind is found from these multi-wavelength observations.

Detailed temporal evolution of this system during its 2019 outburst in optical and radio is being studied by Pavana *et al.* (2020) [in preparation] and in X-rays by Orio *et al.* (2020) and Singh *et al.* (2020).

The optical spectrum obtained from HCT on epoch day 19 (16 September 2019) was modelled to obtain the synthetic spectrum during this phase. The central ionizing source was set to be at effective temperature 2.2×10^5 K and luminosity 2.52×10^{37} erg s^{-1}. The medium consists of one clumpy and two diffuse regions to obtain the modelled spectrum. The optically thick (dense) clump component was used to model most of the lines in the spectrum. Few high ionization lines were fit using non-collisionally excited diffuse region covering 10% of volume. The collisionally excited diffuse component covering 10% of the volume was used to fit the coronal lines in the spectrum. This component was of temperature 4.25×10^6 K and density of 3.98×10^7 cm^{-3}. The estimated abundance values show that iron, nitrogen, calcium, silicon and helium abundances are more than solar, while other abundance values are solar (Table 2). The ejected mass was found to be 5.76×10^{-6} $M_\odot$. The best-fit modelled spectrum (dashed line) with the corresponding observed optical spectrum (continuous line) is as shown in Figure 2. O I (7774 Å, 8446 Å) lines were not modelled due to the limitations of the code. Some of the less prominent Fe II lines have higher χ^2 values and hence influence the total χ^2.

The morphology of the ejecta was obtained using pyCloudy on day 19 (16 September 2019). It was found to be bipolar with equatorial rings and ellipsoidal shell (Figure 3). The equatorial rings became more prominent as the system evolved. Hα and Hβ are present in all the regions. The He I and He II lines are from the inner regions and Fe II from the equatorial

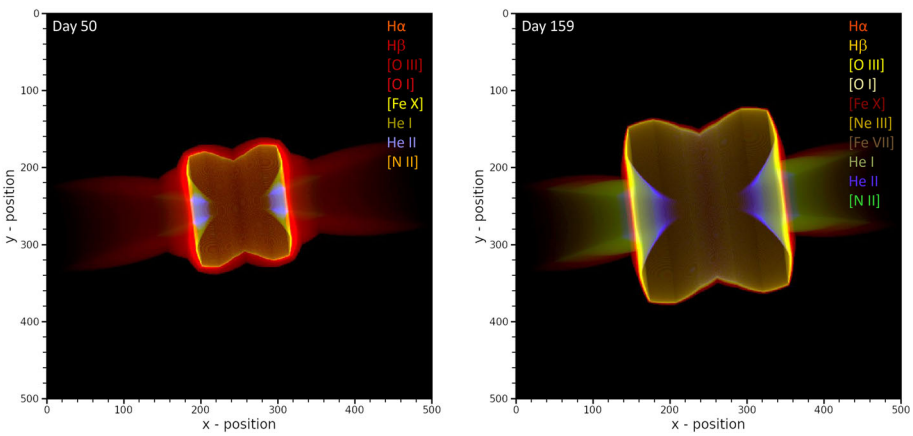

Figure 1. Morphology of the ejecta of RS Oph during its 2006 outburst obtained using the optical spectrum in the two-dimensional plane with *X*-axis being the line-of-sight direction and *Y* being the axis perpendicular to that of the plane of sky and line-of-sight. Here, 1 unit of $x_{50} = y_{50} = 1.35 \times 10^{12}$ cm and $x_{159} = y_{159} = 3.99 \times 10^{12}$ cm. The elemental lines are marked.

Table 2. Chemical abundance values of the V3890 Sgr ejecta at different epochs.

Day	2	7	12	16	19	25	43
$N/N_{\odot}$	1.39	1.43	1.28	1.21	1.23	1.67	2.09
$Si/Si_{\odot}$	1.00	1.28	1.31	1.25	1.25	1.22	1.21
$Fe/Fe_{\odot}$	2.05	1.64	1.71	1.44	1.48	1.34	1.29
$He/He_{\odot}$	1.34	2.14	3.57	4.28	4.65	4.86	6.11
$Ca/Ca_{\odot}$	1.13	1.13	2.26	2.26	1.13	1.13	–

Abundance values are given in the logarithmic scale, relative to hydrogen.

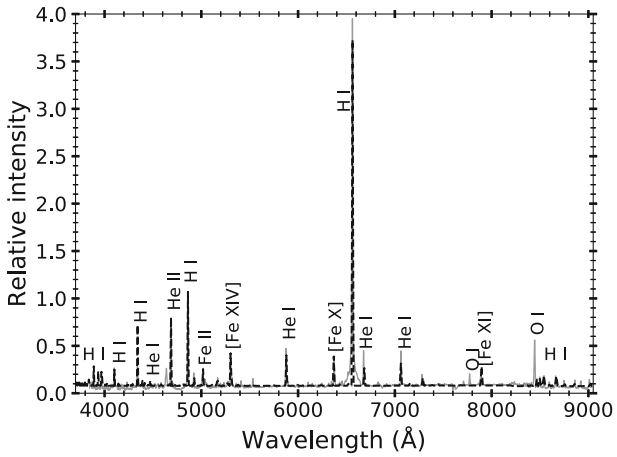

Figure 2. Best-fit modelled spectrum (dash line) plotted over the observed spectrum (continuous lines) for day 19 (16 September 2019) of 2019 outburst of V3890 Sgr.

rings. The coronal lines are coming from the ellipsoidal shell which is 0.35 AU from the red giant surface. The inclination angle of the system was found to $68° \pm 1.35°$.

4. T Pyxidis

The recurrent nova T Pyx has six recorded outbursts, observed in 1890, 1902, 1920, 1945, 1966, and the most recent one in 2011, which was subjected to detailed multi-wavelength studies. Spectral evolution of the 2011 outburst was well studied in the UV, optical and IR wavelengths (Shore *et al.* 2013; Joshi *et al.* 2014; Godon *et al.* 2018; Pavana *et al.* 2019). The very early, pre-maximum spectrum ($\sim$0.8d from outburst discovery) indicates very high ejection velocity of ~ 4000 km s^{-1} that reduced to $\sim 2000-1500$ km s^{-1} by day 2. The spectrum was similar to that of the He/N type of novae. The nature of the spectrum changed from He/N type to Fe II type around maximum, with sharp narrow lines ($\sim 2000-1500$ km s^{-1}). By day 70, the spectrum showed a bluer continuum, and the nature changed back to He/N type. The spectral evolution indicates multiple mass ejection episodes. Surina *et al.* (2014) propose a two phase mass ejection, the first a short-lived (lasting $\sim$6 days) Hubble flow ejection phase occurring immediately after outburst, followed by a more steadily evolving, higher mass loss phase. Multiple absorption systems were seen in the P Cygni profiles during the early phases, that are suggested to be due to the presence of a clumpy wind surrounding the WD (Izzo *et al.* 2012). The nebular spectrum was dominated by high ionization lines with multiple components. T Pyx was detected as a supersoft X-ray source from day 105 to 349. Coincident with the X-ray emission peak detected by the Swift satellite high ionization lines were seen in the optical spectrum, such as [Ne III], [C III], and N III (4640 Å) around day 144. The occurrence of coronal lines like [Fe VII] and [Fe X] was found to be coincident with the supersoft phase, and the peak of radio emission around day 155 (Surina *et al.* 2014). The quiescence spectrum of T Pyx is dominated by the accretion disc spectrum (Anupama 2008; Selvelli *et al.* 2008).

The temporal evolution of the optical spectrum was studied in detail by Pavana *et al.* (2019). The abundance estimates at different epochs estimated them are given in Table 3. Helium, nitrogen, oxygen, and neon were found to have abundance values higher than solar. Iron abundance was found to be higher during the early phase, but solar during the nebular phase, while carbon was nearly solar at all phases. The evolution of the geometry of the shell and elemental distribution during the nebular phase, based on the results by Pavana *et al.* (2019) are shown in Figure 4. The geometry was found to be bipolar conical with equatorial rings, with an inclination angle of $14.75 \pm 0.65°$. It is seen that the oxygen ([O III]) and nitrogen lines arise mainly from the inner regions. Expansion of the equatorial rings is seen in the nebular phase. In the late post-outburst phase, hydrogen and helium lines are found to arise in regions within the nitrogen and oxygen line forming regions, indicating they could be from the accretion disc.

5. U Scorpii

U Sco was discovered to be in its seventh outburst on 2010 Jan 28.4, which has been well studied in all regions from the X-rays to radio. The multi-

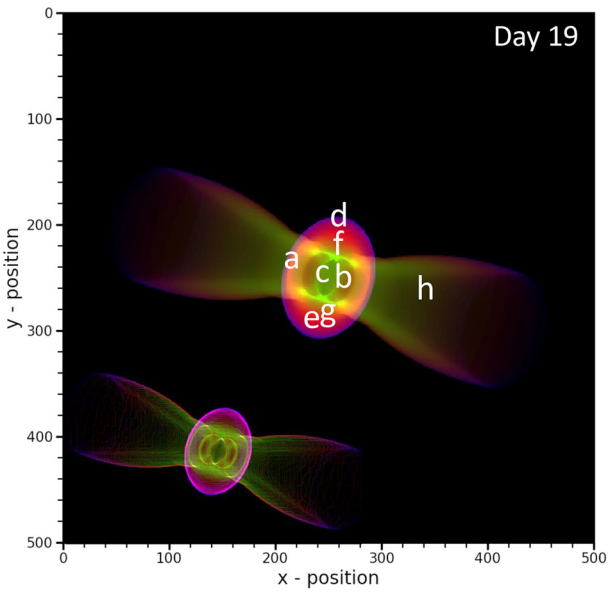

Figure 3. Morphology of the ejecta of V3890 Sgr on day 19 during its 2019 outburst obtained using the optical spectrum in the two-dimensional plane with *X*-axis being the line-of-sight direction and *Y* being the axis perpendicular to that of the plane of sky and line-of-sight. Here, 1 unit of x and y corresponds to 8.13×10^{11} cm. The labels marked represent a: Fe II, b: He I, c: He II, d: [Fe VII], e: [Fe X], f: [Fe XI], g: [Fe XIV], h: H I, i: [N II].

Table 3. Chemical abundance values of the T Pyx ejecta at different epochs.

Day	68	224	252	336	1064
$He/He_{\odot}$	2.00	1.43	1.65	1.16	5.35
$N/N_{\odot}$	5.76	3.02	3.63	2.96	2.78
$O/O_{\odot}$	–	3.01	2.65	2.63	2.21
$Fe/Fe_{\odot}$	1.41	1.09	1.00	1.00	–
$Ne/Ne_{\odot}$	–	3.25	1.36	–	–
$C/C_{\odot}$	1.00	1.00	1.02	1.09	–
$Ca/Ca_{\odot}$	1.13	–	–	–	–

Abundance values are given in the logarithmic scale, relative to hydrogen.

wavelength observations confirm a fast decline, high ejection velocities and an early, short duration supersoft X-ray phase. The outburst spectra (in optical and NIR) are characterized by extremely broad emission lines due to hydrogen Balmer, N III, C III and He I, with initial full width zero intensity velocities of ~ 10000 km s^{-1} (Yamanaka *et al.* 2010; Diaz *et al.* 2010; Kafka & Williams 2011; Anupama *et al.* 2013).

The helium abundance in U Sco is a matter of considerable debate. In the earlier outbursts, Barlow *et al.* (1981), Williams *et al.* (1981), Sekiguchi *et al.* (1988), Munari *et al.* (1999), Anupama & Dewangan (2000) and Evans *et al.* (2001) found helium to be overabundant, with the abundance values (He/H) ranging from 0.4 to 4.5. However, based on an early phase spectrum, Iijima (2002) found a helium abundance of 0.16 during the 1999 outburst. Based on the nebular spectrum during the 2010 outburst, Diaz *et al.* (2010) derived a lower limit to the helium abundance to be in the range 0.1–0.2. Anupama *et al.* (2013) estimated the average helium abundance to be 0.31 ± 0.1 based on multiple epoch spectra, while Maxwell *et al.* (2012) estimated an abundance of 0.073 ± 0.031, based on early phase (days 1.93–12.81) spectra. It thus appears that the abundance estimate is quite heavily dependent on the epoch at which the estimate is made. U Sco is known to be an eclipsing binary with an orbital period of 1.23 days. It is not very clear if the observed abundance variation is also dependent on the orbital period.

6. M31N 2008-12a

M31N 2008-12a is a remarkable RN with eruptions observed since 2008, with an outburst interval of just about one year. It was first discovered during its 2008 eruption by Nishiyama and Kabashima (2008). It has been monitored rigorously and studied in the multi-wavelength regime to understand its short recurrence period and peculiar behaviour (Tang *et al.* 2014; Darnley *et al.* 2015; Henze *et al.* 2015; Darnley *et al.* 2016; Henze *et al.* 2018) from its 2014 outburst onwards.

The optical spectrum obtained from HCT during its 2018 outburst, on day 1.52 (8.61 Nov 2018) was used to model using CLOUDY. The central ionizing source was set at an effective temperature of 1.06×10^5 K and luminosity 10^{37} erg s^{-1}. The medium was assumed to be of a low-density diffuse component and a clump component to obtain a modelled spectrum. The clump hydrogen density was 10^{11} cm^{-3} and diffuse hydrogen density 10^{10} cm^{-3}. The estimated abundance values show that helium was overabundant compared to solar abundance values and the value in the logarithmic scale relative to hydrogen is found to be $He/He_{\odot} = 2.47$. The ejected mass was found to be 7.21×10^{-8} $M_{\odot}$. The best-fit 1D spectrum obtained is shown in Figure 5.

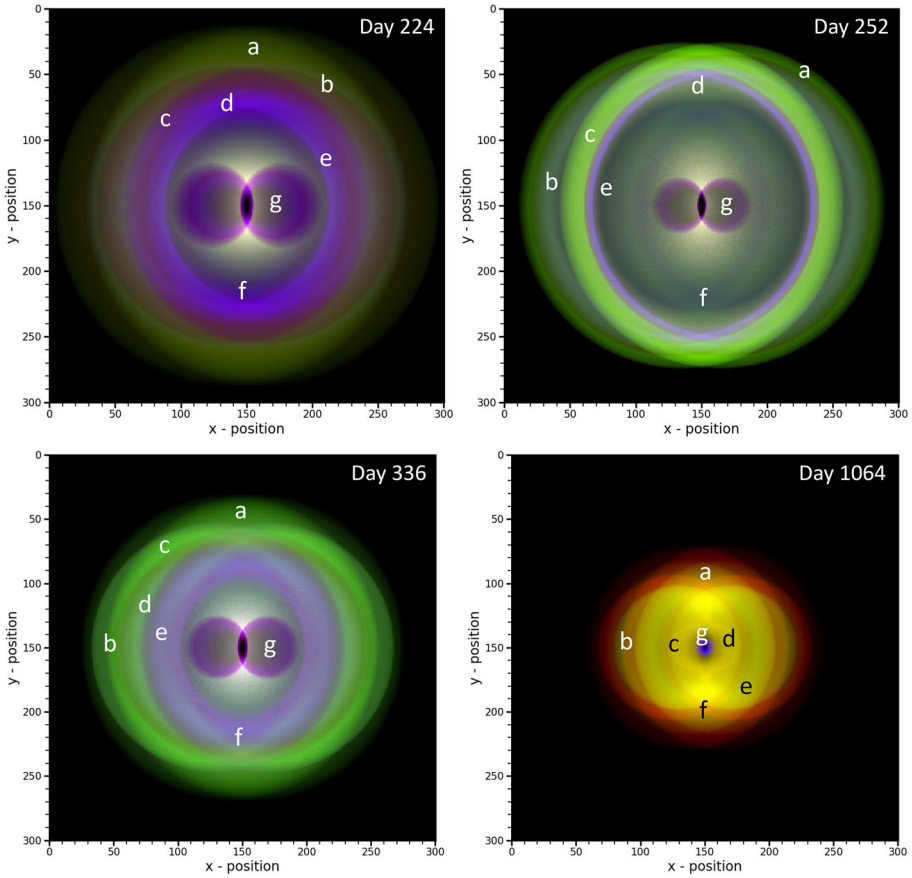

Figure 4. Evolution of the geometry of ejecta of T Pyx on day 224 (*top left*), 252 (*top right*), 336 (*bottom left*), and 1064 (*bottom right*) in the two-dimensional plane with *X*-axis being the line-of-sight direction and *Y* being the axis perpendicular to that of the plane of sky and line-of-sight. The lines corresponding to different colours are marked to show the spatial distribution of emission in the structure. There is formation of multiple equatorial rings and also the spatial distribution of the ionized lines as the system evolves. Here, a: [O III] λ5007, b: [O III] λ4959, c: Hα, d: Hβ, e: N III λ4638, f: [N II] λ5755, g: He II λ4686. Only dominant lines are marked. Here, 1 unit of *x* and *y* position correspond to $x_{224} = 6.3 \times 10^{12}$ cm, $x_{252} = 1.41 \times 10^{13}$ cm, $x_{336} = 2.09 \times 10^{13}$ cm, and $x_{1064} = 1.66 \times 10^{12}$ cm.

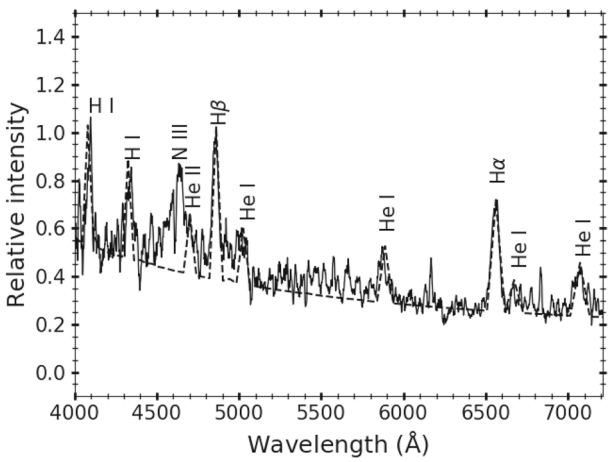

Figure 5. Best-fit modelled spectrum (dash line) plotted over the observed spectrum (continuous line) for day 1.52 (8.61 Nov 2018) of 2018 outburst of M31N 2008-12a.

The morphology of the ejecta using pyCloudy was found to be bipolar one with cones and an equatorial ring inclined at an angle of $81^\circ \pm 1.53^\circ$. The He I and He II lines come from the bipolar conical components (inner regions), and the hydrogen lines come from all the regions. [N II] arises mainly from the equatorial ring (Figure 6).

7. Summary

The abundances of elements corresponding to the most prominent lines in the spectra of a few recurrent novae are discussed here, together with their distribution in the ejecta. In all the cases discussed here, helium, oxygen, and nitrogen are found to be over-abundant in the nova ejecta during the outburst phase, while they are almost solar at quiescence, clearly

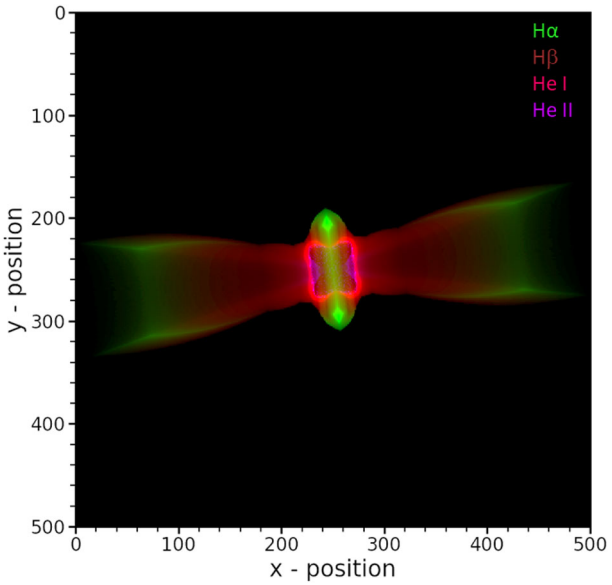

Figure 6. Morphology of the ejecta of the 2018 outburst of M31N 2008-12a obtained on day 1.52 using the optical spectrum. It is plotted in the two-dimensional plane with *X*-axis being the line-of-sight direction and *Y* being the axis perpendicular to that of the plane of sky and line-of-sight. The lines corresponding to different colours are marked to show the spatial distribution of emission in the structure. Here, 1 unit of *x* and *y* correspond to 2.26×10^{10} cm.

indicating the production of these elements during TNR reactions at outburst. All the novae show a temporal evolution of the abundances. This temporal evolution could be due to the changing physical conditions in the line emitting regions of the expanding nova shell leading to varying ionization fractions. Enhanced bipolar nature is seen in all the novae except for T Pyx. Cones are the closest component to the central source in all the novae. It is usually formed due to emission from nitrogen, helium and hydrogen lines. The equatorial rings are either due to Fe II or oxygen emission. The elemental distribution provides clues to the nature of the shell ejection during the outburst. The results presented here emphasize the need for detailed spectroscopic monitoring of these systems during outburst as well as quiescence.

Acknowledgements

The support of the staff at IAO, CREST and VBO during observations is acknowledged.

References

Anupama, G. C. 2008, ASP Conf. Ser., 401, 31
Anupama, G. C. 2013, in IAU Symp. 281, Binary Paths to Type Ia Supernovae Explosions, Cambridge Univ. Press, Cambridge, 154
Anupama, G. C., Dewangan, G. C. 2000, AJ, 119, 1359
Anupama G. C., Kamath U. S., Ramaprakash A. N., *et al.*, 2013, A&A, 559, A121
Barlow, M. J., Brodie, J. P., Brunt, C. C., *et al.* 1981, MNRAS, 195, 61
Bode M. F. *et al.*, 2006, ApJ, 652, 629
Cao Y., *et al.*, 2015, Nature, 521, 328
Darnley, M. J., Henze, M., Steele, I. A., *et al.* 2015, A&A, 580, A45
Darnley, M. J., Henze, M., Bode, M. F., *et al.* 2016, ApJ, 833, 149
Diaz, M. P., Williams, R. E., Luna, G. J., Moraes, M., Takeda L. 2010, AJ, 140, 1860
Dilday B., *et al.*, 2012, Science, 337, 942
Evans, A., Krautter, J., Vanzi, L., Starrfield, S. 2001, A&A, 378, 132
Ferland, G. J., Chatzikos, M., Guzmán, F., *et al.* 2017, Revista Mexicana de Astronoma y Astrofsica, 53, 385
Godon, P., Sion, E., Williams, R., Starrfield, S. 2018, AJ, 862, 89
Henze, M., Ness, J.-U., Darnley, M. J., *et al.* 2015, A&A, 580, A46
Henze, M., Darnley, M. J., Williams, S. C., *et al.* 2018, ApJ, 857, 68
Iijima, T. 2002, A&A, 387, 1013
Izzo, L., Ederoclite, A., Della Valle, M., *et al.* 2012, Mem. Soc. Astron. It., 83, 830
Joshi, V., Banerjee, D. P. K., Ashok, N. M. 2014, MNRAS, 443, 559
Kafka, S., Williams, R. 2011, A&A, 526, A83
Kantharia N. G., Anupama G. C., Prabhu T. P., Ramya S., Bode M. F., Eyres S. P. S., O'Brien T. J., 2007, ApJ, 667, L171
Kasen D., 2010, ApJ, 708, 1025
Khokhlov A. M., 1991, A&A, 245, 114
Maoz, D., & Graur, O. 2017, ApJ, 848, 25
Maxwell, M. P., Rushton, M. T., Darnley, M. J., *et al.* 2012, MNRAS, 419, 1465
Mondal, A., Anupama, G. C., Kamath, U. S., *et al.* 2018, MNRAS, 474, 4211
Mondal, A., Das, R., Anupama, G. C., Mondal, S. 2020, MNRAS, 492, 2326
Morisset, C. 2013, pyCloudy: Tools to manage astronomical Cloudy photoionization code, Astrophysics Source Code Library
Munari, U., Zwitter, T., Tomov, T., *et al.* 1999, A&A, 347, L39
Narumi H., Hirosawa K., Kanai K., Renz W., Pereira A., Nakano S., Nakamura Y., Pojmanski G., 2006, IAU Circ., 8671, 1

Nishiyama, K. & Kabashima, F. 2008, CBATIAU, http://www.cbat.eps.harvard.edu/iau/CBAT_M31.html#2008-12a
Orio, M., Drake, J, Ness, J.-U., *et al.*, 2020, ApJ, 895, 80
Patat F., Chugai N. N., Podsiadlowski P., Mason E., Melo C., Pasquini L., 2011, A&A, 530, A63
Pavana, M., Anche, R. M., Anupama, G. C., Ramaprakash, A. N., & Selvakumar, G. 2019, A&A, 622, A126
Pavana, M. *et al.*, 2020, [under preparation]
Phillips M. M., 1993, ApJ, 413, L105
Schaefer, B. E. 2010, ApJS, 187, 275
Sekiguchi, K., Feast, M. W., Whitelock, P. A., *et al.* 1988, MNRAS, 234, 281
Selvelli, P., Cassatella, A., Gilmozzi, R., & Gonzlez-Riestra, R. 2008, A&A, 492, 787
Shore, S. N., Schwarz, G. J., De Gennaro Aquino, I., *et al.* 2013, A&A, 549, A140
Singh, K. P., Grish, V., Pavana. M., Noss, J-U., Anupama, G. C., Odam, M., 2020, MNRAS (in press)
Skopal A. *et al.*, 2008, in Evans A., Bode M. F., O'Brien T. J., Darnley M. J., eds, ASP Conf. Ser. Vol. 401, RS Ophiuchi (2006) and the Recurrent Nova Phenomenon, Astron. Soc. Pac., San Francisco, p. 227
Sokoloski J. L., Luna G. J. M., Mukai K., Kenyon S. J., 2006, Nature, 442, 276
Starrfield, S., Iliadis, C., Timmes, F. X., *et al.* 2012, BASI, 40, 419
Starrfield S., Bose M., Iliadis C., Hix W. R., Woodward C. E.,Wagner R. M., 2020, ApJ, 895, 70
Surina, F., Hounsell, R. A., Bode, M. F., *et al.* 2014, AJ, 147, 107
Tang, S., Bildsten, L., Wolf, W. M., *et al.* 2014, ApJ, 786, 61
Woosley S. E., Weaver T. A., 1994, ApJ, 423, 371
Williams, R. E., Sparks, W. M., Gallagher, J. S., *et al.* 1981, ApJ, 251, 221
Yamanaka, M., Uemura, M., Kawabata, K. S., *et al.* 2010, PASJ, 62, L37